Journal of Alloys and Compounds 509 (2011) 4861–4867

Contents lists available at ScienceDirect

Journal of Alloys and Compounds

journal homepage: www.elsevier.com/locate/jallcom

Negative magnetization, magnetic anisotropy and magnetic ordering studies on Al^{3+}-substituted copper ferrite

V.K. Lakhani [a], Bangchuan Zhao [b], Lan Wang [b], U.N. Trivedi [a], K.B. Modi [a,*]

[a] Department of Physics, Saurashtra University, Rajkot 360005, India
[b] School of Physical and Mathematical Sciences, Nanyang Technology University, Singapore 637371, Singapore

ARTICLE INFO

Article history:
Received 19 August 2010
Received in revised form 24 January 2011
Accepted 27 January 2011
Available online 22 February 2011

Keywords:
Ferrites
Magnetic properties
Magnetic anisotropy
Magnetic ordering

ABSTRACT

Detailed magnetic properties of Al^{3+}-modified $CuFe_2O_4$ spinel ferrite system: $CuAl_xFe_{2-x}O_4$; $x = 0.0, 0.2, 0.4$ and 0.6, have been studied by means of X-ray powder diffraction, field cooled (FC) and zero field cooled magnetization (ZFC) ($H = 10$ mTesla, $T = 4$–325 K), magnetic hysteresis ($H_{max} = 2$ Tesla, $T = 10$ and 300 K) and low field (40 A/m) ac susceptibility ($T = 300$–750 K) measurements. The system exhibits canted spin structure. It has been shown that the observed features of the FC–ZFC magnetization and ac susceptibility curves arise due to the low magneto crystalline anisotropy, not due to the cluster spin-glass-like magnetic ordering. The interesting features like low temperature cusp in the ZFC magnetization for all the compositions and negative magnetization for $x = 0.6$ composition have been observed. An attempt has been made to explain the negative magnetization within the framework of available models.

1. Introduction

Copper ferrite ($CuFe_2O_4$) is one of the most investigated ferrite by various experimental techniques. Due to a relatively small energy difference between Cu^{2+}-ions at the tetrahedral (A-) and octahedral (B-) sites, cation redistribution is possible and strongly dependent on the annealing temperature, cooling rate, microstructure and other parameters [1]. Copper ferrite is mostly an inverse spinel. Statistically, 6–24% of Cu^{2+} ions occupy the A-sites depending on the preparative parameters [2]. The corresponding magnetization is about 1.48–2.92 μ_B per chemical formula. On the other hand, copper ferrite is ferrimagnetic at room temperature with Neel temperature of 738 K [3], although lower values down to 290 K have also been reported [2]. Thus, tailoring of the magnetic and electrical properties of $CuFe_2O_4$ is possible with ease [1,4,5]. On the spin structure, as the t_2g bands of Cu^{2+} on the B-sites are fully occupied; the inter-site direct hopping is absent and results in a ferromagnetic or weak anti-ferromagnetic exchange coupling between the B-sites which stabilize the Neel configuration (collinear spin arrangement). However, as Cu^{2+} is redistributed on the A-sites, Fe^{3+} occupies the B-sites and results in an anti-ferromagnetic exchange coupling between the B-sites, which frustrates the Neel configuration. If the exchange coupling between Cu^{2+} on the A-sites and Fe^{3+} on the B-sites is weak enough, the redistribution may result in spin canting, or other complex structures. In addition, redistribution of Cu^{2+} from the B- to A-sites alters the ground multiple from doublet to triplet. This effect, combined with the large spin-orbital coupling constant, may result in different magnetocrystalline anisotropy [6].

In particular, copper ferrite ($CuFe_2O_4$) in bulk polycrystalline [7,8] and thin film [5,9–12] forms have shown very interesting multifunctional properties upon the application of external stimuli. On the other hand, nanoparticles of $CuFe_2O_4$ have been shown to be useful as a catalyst for CO_2 decomposition, hydrogen production and as a gas sensor [13]. In the literature, wide varieties of experimental techniques have been employed for the synthesis and characterization of nanocrystalline copper ferrite [14–19].

The substitution of Al^{3+}-ions have some beneficial effects on power handling capability [20]. The addition of Al^{3+}-ions have shown to modify the structural properties [21], electrical properties [22,23] including switching characteristics [7,24], magnetic properties [22,25–29], dielectric properties [30,31], and elastic properties [32] of spinel ferrite materials in an interesting manner.

The system under investigation, copper ferrite aluminates, $CuAl_xFe_{2-x}O_4$, belong to a large class of compounds having the general formula $A^{2+}B_2{}^{3+}O_4{}^{-2}$ and crystallize in the spinel structure.

Magnetic systems undergoing transitions to ordered ferromagnetic, anti-ferromagnetic and ferrimagnetic states are reported to show irreversibility, indicated by the difference between their field cooled (FC) and zero-field cooled (ZFC) magnetization [33,34]. The irreversible FC and ZFC magnetic behavior is one of the characteristic features of a spin glass [35,36], other characteristic properties of a spin glass include the relaxation of magnetization (i.e. the aging effect) and the presence of a cusp in the low field ZFC magnetiza-

* Corresponding author. Tel.: +91 281 2588428; fax: +91 281 2576802.
E-mail address: kunalbmodi2003@yahoo.com (K.B. Modi).

0925-8388/$ – see front matter © 2011 Elsevier B.V. All rights reserved.
doi:10.1016/j.jallcom.2011.01.190

tion as well as in the thermal variation of ac susceptibility curves. The spins are frozen in random directions due to lack of long-range magnetic interactions. Spin-glass-like properties have been reported for magnetic systems [37,38] for which neutron diffraction studies indicate long range magnetic ordering. These results contradict each other. On the other hand, low field magnetic behavior of some ferromagnetic and ferrimagnetic oxides indicated that their spin-glass-like magnetic properties originate from the magnetocrystalline anisotropy [33,39]. In other words, the magnetic behavior similar to that of cluster spin glass could also be explained based on the magneto-crystalline anisotropy of the compound. Though, conventional spin glasses and materials showing spin-glass-like features such as superparamagnetic systems, cluster spin glass systems, superconducting oxides, the ordered magnetic system, show thermomagnetic irreversibility between the FC and ZFC magnetization and cusp in their ZFC susceptibilities, the origin of such a behavior is not yet properly understood [33].

Recently, Sundaresan et al. [40] have demonstrate that in certain ferrimagnetic materials, small negative trapped field in the sample space as well as large coercive fields are responsible for the observed negative magnetization under ZFC process. The negative values of magnetization measured in low applied fields for double perovskite composition: $LaSrCoRuO_6$, have been interpreted to be due to disorder in site occupancy of Co and Ru leading to octahedral distortions and formation of Ru–O–Ru ferromagnetic linkages. It is mentioned that below 150 K these ferromagnetic Ru spins polarize the Co-spins in a direction opposite to that of the applied field resulting in observed negative magnetization [41]. In short, there still exists large controversy regarding the origin of the phenomenon. A microscopic understanding of this phenomenon can be effectively utilized to tailor the magnetic properties for various applications. This would facilities the design of various magnetic memories, thermo magnetic switches and magnetic cooling/heating devices [42]. The authors have observed a crossover of the ZFC magnetization from positive to negative for the $CuAl_{0.6}Fe_{1.4}O_4$ ($x = 0.6$) composition, below their magnetic ordering temperature.

The thermomagnetic irreversibility ($M_{FC} > M_{ZFC}$) below a certain temperature has been observed for many ferrite system in nanoregime [43,44]. The results are explained based on the blocking of the magnetic moment of nanoparticles and the superparamagnetic behavior of the studied system. It may also be due to the large anisotropy barrier for the studied compositions. On the other hand, the observed non-coincidence of the FC–ZFC curves for nanosized nickel ferrite with grain size of 51 nm, has been explained based on the distribution of particle size in the sample [45]. We have observed that for $x = 0.0$,0.4 and 0.6 compositions of $CuAl_xFe_{2-x}O_4$ system, the ZFC and FC curves bifurcate at about 276, 310 and 278 K, respectively, while for $x = 0.2$ composition, ZFC–FC curves do not coincide throughout the temperature range studied. Nanosized ferrite particles exhibit unusual magnetic properties which are not observed in the bulk material, such as, single domain behavior, superparamagnetism, and reduced magnetization. Similarly, the mechanisms responsible for such magnetic behavior of ferrite nanoparticles are not directly applicable to coarse-grained (micron size particles) polycrystalline ferrite material.

In the present communication, it clearly demonstrates that the observed features of the FC–ZFC magnetization and ac susceptibility curves arise due to the low magnetocrystalline anisotropy, but not due to the cluster-spin-glass-like phase in the system. To our knowledge, no work has been reported on the role of magnetocrystalline anisotropy in governing the magnetic properties of the coarse-grained ferrite materials in general, except for an excellent work by Joy et al. [33,46] on Ni–Zn ferrite, $Ni_{0.8}Zn_{0.2}Fe_2O_4$. Recently, the role of anisotropy ion, Fe^{2+}, in enhancing and tailoring the magnetization of $CuFe_2O_4$ nanoparticles has been discussed by Thapa et al. [13], while the observed large magnetic moment (80 A m^2/kg) for nanosized $Cu_{0.25}Co_{0.25}Zn_{0.5}Fe_2O_4$ has been explained in terms of the enhancement in the B–B interaction because of the distortion in the B-sites due to the presence of the Jahn–Teller cation Cu^{2+} at this site [47].

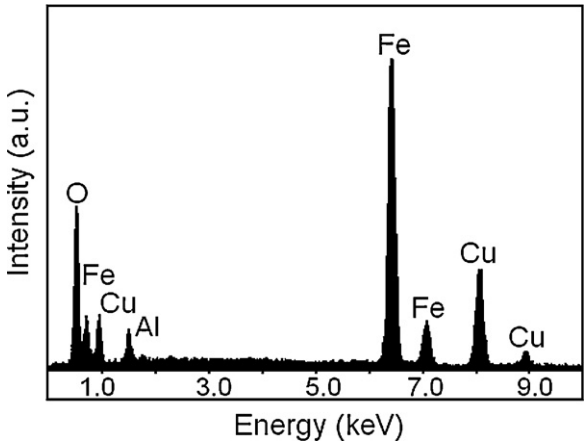

Fig. 1. EDAX pattern of $CuAl_{0.4}Fe_{1.6}O_4$ ($x = 0.4$) composition.

To our knowledge few research reports are available on various physical properties of $CuAl_xFe_{2-x}O_4$ spinel ferrite system including our recent work on the system [21,25,26,30,32,48–51].

In the view of above facts, the effect of Al^{3+} substitution on magnetic properties of $CuFe_2O_4$ with general chemical formula: $CuAl_xFe_{2-x}O_4$ ($x = 0.0$, 0.2, 0.4 and 0.6) have been studied by means of field cooled and zero field cooled magnetization, magnetic hysteresis and low field ac susceptibility measurements.

2. Experimental

From the CuO-Fe_2O_3 phase-diagram, $CuFe_2O_4$ is formed between 1000 and 1100 °C. The samples sintered below 1000 °C or above 1100 °C were of mixed-phase [4]. Aluminum (Al^{3+})-modified copper ferrite ceramics with a general formula of $CuAl_xFe_{2-x}O_4$ ($x = 0.0$, 0.2, 0.4 and 0.6) were synthesized from high purity chemicals, namely CuO, Al_2O_3 and Fe_2O_3, of 99.9% purity supplied by Sigma–Aldrich. The oxides were mixed thoroughly in stoichiometric proportions to yield the desired composition and then wet-ground. The mixture was dried and pressed into pellets. These pellets were pre-sintered at 1100 °C for 24 h and slowly cooled to room temperature. The samples were again powdered, pressed into pellets, sintered at 1100 °C for 24 h and then slowly furnace cooled to room temperature at the rate of 2 °C/min. The stoichiometry of the powder samples was checked by energy dispersive analysis of X-rays (EDAX). The samples were characterized for single phase formation and the determination of cation distributions by X-ray powder diffractometry using Cu Kα radiation at 300 K.

Magnetic measurements (field-cooled (FC) and zero-field-cooled (ZFC) magnetization and magnetic hysteresis) were performed using the physical property measurement system (PPMS, Quantum Design). The low field ac susceptibility measurements for powdered samples were made in the temperature range 300–750 K using double coil setup [52], operating at a frequency of 263 Hz with r.m.s. field of 40 A/m.

3. Results and discussion

High temperature prolonged sintering may result in the loss of ingredients, which leads to non-stoichiometry in composition. This, in turn, shows unexpected behavior which cannot be explained based on normal stoichiometry. Thus, it was essential to check the chemical stoichiometry of each composition. A representative energy dispersive analysis of X-rays (EDAX) pattern for typical composition with $x = 0.4$ is shown in Fig. 1.

The results of EDAX confirm the expected stoichiometry, with small oxygen deficiency. No trace of any impurity was found indicating the purity of the samples. It is also clear that there is no loss of any ingredient after high temperature sintering. EDAX results suggest that the precursors have fully undergone the chemical reaction

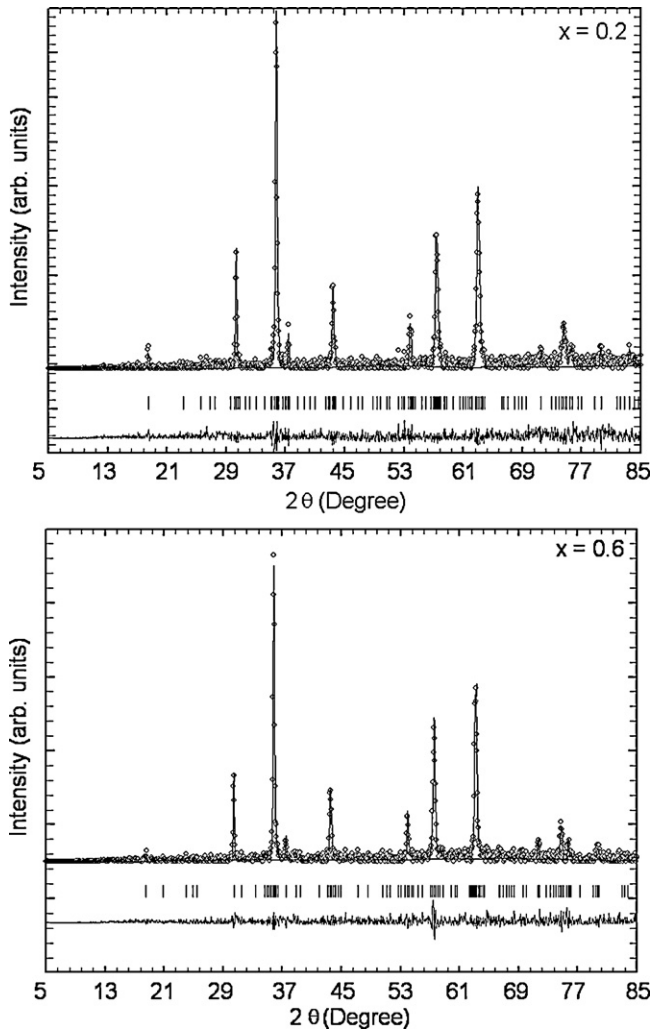

Fig. 2. Observed (solid circles) and calculated (solid line) X-ray powder diffraction patterns for the $CuAl_xFe_{2-x}O_4$ ($x = 0.2$ and 0.6) system at 300 K. The difference between the observed and calculated spectra is plotted at the bottom. The ticks indicate allowed Bragg peaks positions.

to form the expected ferrite composition. The reason for making EDAX characterization was to verify the purity and the chemical composition.

The room temperature (300 K) X-ray diffraction (XRD) patterns of the samples were obtained by X-ray powder diffractometry. Indexing and Rietveld refinement using general scattering analysis software (GSAS) of XRD patterns for $x = 0.0, 0.2, 0.4$ and 0.6 compositions of $CuAl_xFe_{2-x}O_4$ system, revealed that these are single-phase compounds, crystallizing in a face centered cubic (fcc) structure (space group O^7_h $Fd3m$). No peaks from impurity phases could be detected within the limits of X-ray detection, which is typically 5%. Fig. 2 displays Rietveld fitted XRD patterns for the typical compositions with $x = 0.2$ and 0.6. One of the most important Rietveld error indices or discrepancy values is that of "Chi-squared" or χ^2 [53]. It is found that χ^2 for different compositions lie in the range 1.2–1.4. The χ^2 values obtained in the present analysis suggest good refinements of the data.

The distribution of the cations among the available tetrahedral (A-) and octahedral (B-) sites of the spinel lattice have been determined by comparing experimental and calculated intensities of the diffracted beam. The X-ray diffraction line intensities of various Bragg's planes were calculated for different combinations of the cations in the A- and B-sites using a computer program based

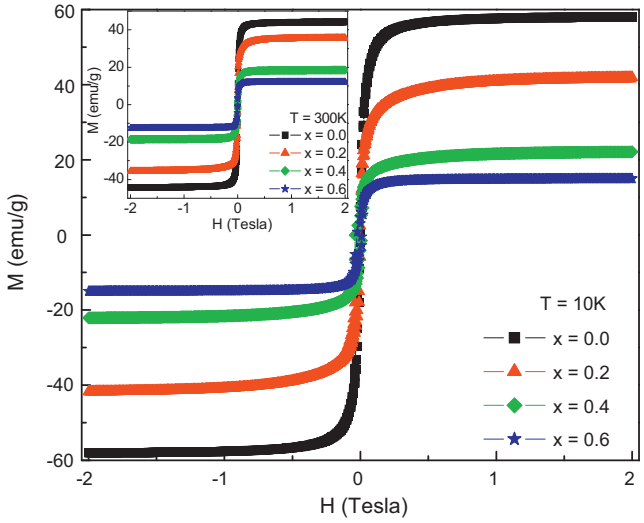

Fig. 3. Magnetic field dependence of magnetization at 10 K; main panel, inset at 300 K, for Cu–Fe–Al–O samples.

on the Buerger formula [54]. In the process of arriving at the final cation distribution, the site occupancy of all the cations was varied for many possible combinations and those that agree well with the experimental intensities of various Bragg's planes were taken into consideration. The cation distributions obtained for $CuAl_xFe_{2-x}O_4$ system are represented as:

$x = 0.0$ $(Cu_{0.22}Fe_{0.78})[Cu_{0.78}Fe_{1.22}]O_4$

$x = 0.2$ $(Cu_{0.22}Fe_{0.70}Al_{0.08})[Cu_{0.78}Fe_{1.10}Al_{0.12}]O_4$

$x = 0.4$ $(Cu_{0.18}Fe_{0.64}Al_{0.18})[Cu_{0.82}Fe_{0.96}Al_{0.22}]O_4$

$x = 0.6$ $(Cu_{0.14}Fe_{0.58}Al_{0.28})[Cu_{0.86}Fe_{0.82}Al_{0.32}]O_4$

Near room temperature (323 K) Seebeck coefficient values (α) have been used to determine the cationic concentration of Cu^{1+}, Cu^{2+}, Fe^{2+} and Fe^{3+} ions using the Heikes formula [55]. The details of this are given elsewhere [51]. The actual cation distributions thus derived for different compositions are summarized below, which, in turn, are used to explain the magnetic properties.

$x = 0.0$ $(Cu^{1+}_{0.15}Cu^{2+}_{0.07}Fe^{3+}_{0.78})^A[Cu^{2+}_{0.78}Fe^{3+}_{1.22}]^B O^{2-}_{3.925}$

$x = 0.2$ $(Cu^{1+}_{0.12}Cu^{2+}_{0.10}Fe^{3+}_{0.70}Al^{3+}_{0.08})^A[Cu^{2+}_{0.78}Fe^{3+}_{1.10}Al^{3+}_{0.12}]^B O^{2-}_{3.940}$

$x = 0.4$ $(Cu^{2+}_{0.18}Fe^{3+}_{0.64}Al^{3+}_{0.18})^A[Cu^{2+}_{0.82}Fe^{2+}_{0.43}Fe^{3+}_{0.53}Al^{3+}_{0.22}]^B O^{2-}_{3.785}$

$x = 0.6$ $(Cu^{2+}_{0.14}Fe^{3+}_{0.58}Al^{3+}_{0.28})^A[Cu^{2+}_{0.86}Fe^{2+}_{0.35}Fe^{3+}_{0.47}Al^{3+}_{0.32}]^B O^{2-}_{3.825}$

The main plot of Fig. 3 shows the magnetization (M) versus applied magnetic field (H) curves, measured at 10 K for $x = 0.0$–0.6 compositions. The hysteresis loops recorded at 300 K are shown in the inset. The values of saturation magnetization (σ_s), and the magneton number (saturation magnetization per formula unit in Bohr magneton (μ_B)) at 10 K for each composition are listed in Table 1. Fig. 3 demonstrates that there is a high field slope to magnetization $M(H)$ curves for $x = 0.0$–0.6, compositions which exhibit strong evidence for a canted spin structure, and canting angle varies with applied field. The high field slope has been established as due to the high magnetic anisotropy [56]. This fact does not apply here since all the compositions have very low concentration of magnetic anisotropy ion (Fe^{2+}), and therefore, the observed features may be thought of arising from canting of spins. From the field dependence

Table 1
Magnetic parameters for $CuAl_xFe_{2-x}O_4$ system.

Al-content (x)	σ_s (emu/g)	n_B (μ_B)	n_B^N (μ_B)	$\langle\theta_{RCS}\rangle$ (°)	J_{AB}/J_{BB}	T_{cusp} (K)	T_{irr} (K)
0.0	58.07	2.49	2.91	20.1	1.63	60	276
0.2	41.71	1.74	2.68	31.8	1.48	65	–
0.4	22.61	0.92	1.81	34.1	1.27	61	310
0.6	15.22	0.61	1.57	37.7	1.20	75	287

of magnetization, and observed magnetic moment, it is clear that the samples with $x = 0.0$–0.6 show ferrimagnetic behavior, which decreases with increasing x values.

A very important characteristic of the $M(H)$ curves is the negligible coercivity and remanence for all the compositions, which are often found in magnetic cluster system [57]. The negligible coercivity for different compositions also suggests that these are low anisotropic compounds [46].

According to the Neel's two sub-lattice model of ferrimagnetism [58], Neel's magnetic moment per formula unit in μ_B, n_B^N, is expressed as:

$$n_B^N = M_B(x) - M_A(x) \quad (1)$$

where M_B and M_A are the octahedral (B-) and tetrahedral (A-) sub-lattice magnetization to be determined from the cation distributions and the free-ion magnetic moments of the cations involved: $m(Fe^{3+}) = 5\,\mu_B$, $m(Fe^{2+}) = 4\,\mu_B$, $m(Cu^{2+}) = 1\,\mu_B$, $m(Cu^{1+}) = 0\,\mu_B$ and $m(Al^{3+}) = 0\,\mu_B$. It is clear from the Table 1, that the observed values of magneton number do not agree with the Neel's moment (n_B^N) found from the Neel's formula for collinear spin arrangement. This indicates significant canting of the B-site moments. The substitution of non-magnetic Al^{3+} ions in $CuFe_2O_4$ may lead to collapse of long range magnetic ordering in the system. Therefore, it was thought appropriate to apply random canting of spins (RCS) model. Since, the actual spin canting depends upon a number of non-magnetic nearest neighbours and their spatial arrangement, the statistical model like RCS proposed by Rosenewaig [59] should be used. According to this model, the B-sites magnetic ions can be considered to be canted with an average angle $\langle\theta_{RCS}\rangle$ due to non-magnetic substitution (Al^{3+}) which, in the average nearest neighbour approximation is estimated to be:

$$\cos\langle\theta_{RCS}\rangle = \left(\frac{M_A}{M_B}\right)\left(\frac{J_{AB}}{A_{BB}}\right) \quad (2)$$

where J_{AB} and J_{BB} are exchange integrals.

The net magnetization per formula unit (magneton number), n_B, is related to canting angle, $\langle\theta_{RCS}\rangle$, by:

$$n_B = M_B(x)\cos\langle\theta_{RCS}\rangle - M_A(x) \quad (3)$$

The experimental values of canting angle, $\langle\theta_{RCS}\rangle$ have been obtained from Eq. (3), using measured n_B values (Table 1), and the same are also listed in Table 1.

As the Al^{3+}-content increases in the system, the magnetic coupling, J_{AB}/J_{BB}, remains nearly constant for $x = 0.0$–0.2 and thereafter it is getting weakened for $x > 0.2$, indicates change in the magnetic structure (increase frustration and disorder).

Further, studies on magnetic properties using dc magnetization measurements were carried out. Fig. 4 shows plots of magnetization versus temperature (M–T) recorded in zero-field cooled (ZFC) and field cooled (FC) modes in an external magnetic field of 10 mT for the samples with $x = 0.0$, 0.2, 0.4 and 0.6. The ZFC magnetization was recorded by first cooling the sample from 325 to 4 K in zero magnetic fields, then applying the magnetic field and warming the sample up to 325 K in the presence of the field and recording the moment during the warming cycle. Field cooled patterns were obtained by first cooling the sample from 325 K down to 4 K in the external field and then warming it up to 325 K and

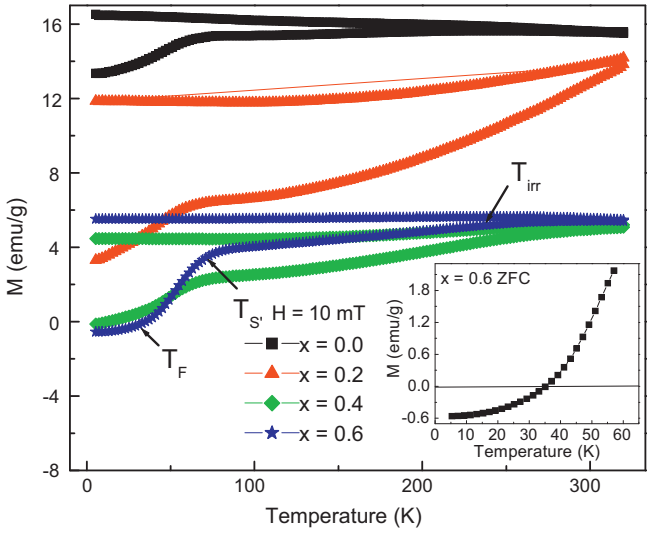

Fig. 4. Temperature dependence of M_{FC} and M_{ZFC} of Cu–Fe–Al–O system. Inset shows the expanded version of the ZFC mode near the magnetic transition.

recording the moment. The plots of ZFC–FC magnetization show thermo-magnetic irreversibility (TMI) (divergence between FC and ZFC magnetization). This is the property of all magnetic systems exhibiting magnetic hysteresis behavior. For the compositions with $x = 0.0$, 0.4 and 0.6 the ZFC and FC curves bifurcate at about 276, 310 and 287 K, respectively. This temperature is referred to as the temperature of irreversibility above which $[(M_{FC}/M_{ZFC}) - 1]$ is less than 1%. The behavior of $x = 0.2$ composition is particularly interesting of which ZFC and FC curves show bifurcation at the whole temperature range, which indicates that the system is not magnetically homogeneous although the material is chemically homogeneous. This may indicate the existence of magnetic cluster phase in the sample [57].

During both the FC and the ZFC processes, the anisotropy field plays an important role in determining the magnetization at a given field strength. Magneto crystalline anisotropy aligns the spins in a preferred direction. As mentioned earlier, during the process of zero-field cooling (ZFC) magnetization measurement, no magnetic field is applied while cooling the sample through the ordering temperature. At the lowest temperature when a small magnetic field is applied, the magnitude of resultant magnetization will depend on the magnetic anisotropy of that material. If the system is low anisotropic, as in the present case, the small applied magnetic field will be sufficient to rotate the spins in the direction of the applied field and therefore the magnetization will be very large, i.e. difference in the FC and ZFC magnetization will be small. If the anisotropy of the sample is very low, the FC magnetization will remain almost constant, while the FC magnetization increases with decreasing temperature for highly anisotropic materials [33]. The observed flat response of FC magnetization with temperature confirms that all the ferrite compositions studied are low anisotropy materials.

We have observed a very broad hump in the ZFC magnetization (M_{ZFC}) for $x = 0.0$, 0.4 and 0.6 compositions in vicinity to bifurcate temperature between the FC and ZFC curves. The sharp peak in M_{ZFC} is observed at a temperature where the coercivity is larger than the applied field and a broad maximum is observed when coercivity is comparable or smaller than the applied field. This observation suggests that in the present case coercivity for different compositions is much less than the 10 mT and materials under study are low anisotropy compounds.

The TMI between the M_{FC} and M_{ZFC} and a very broad maximum in the ZFC magnetization of the ferrite compositions are due to their

magnetic anisotropy and not due to any spin-glass-like behavior as reported for many ordered magnetic systems [46].

A careful examination of Fig. 4, reveals two interesting features: (i) for $x = 0.6$ composition ZFC magnetization decreases slowly with decrease in temperature, shows cusp centered around 75 K, then decreases rapidly, passes through a zero value of magnetization ($M = 0$) at the compensation temperature ($T \sim 35$ K). Below this temperature, the magnetization is negative, down to the lowest temperature (4 K).

Negative magnetization was observed more than five decades ago in spinel-like Co_2VO_4 [60], and more recently in natural ferrites such as magnetite and maghemite [61] spinel-like $CoCr_2O_4$ and $MnCr_2O_4$ [62], ferrite-like $Fe_2Mo_{0.6}Ti_{0.4}O_4$ [63], perovskite-like $NdMnO_{3+\delta}$ $La_{0.75}Nd_{0.25}CrO_3$ [64], molecular magnets [65], other oxides [66], double perovskites Sr_2YbRuO_6 [67], Cu, Mn and Fe based prussian blue analogues [42], Co_2CrAl type Heusler alloy, inorganic compounds [68] and $CuFe_2O_4$ thin film [69]. A number of mechanisms and new models have been proposed to explain the phenomenon of negative magnetization [64]. Usually, negative magnetization appears in complex ferri or canted antiferromagnetic systems or two-phase magnetic system.

Since, a non-zero, but negative residual field of the superconducting magnet during cooling is another possible reason for the observed diamagnetism, we have checked the residual field. It was +2.5 Oe, which is positive. Therefore, the observed negative magnetization is not due to the residual field of SQUID magnetometer during cooling. Furthermore, the investigated sample is ferrite sample; we can safely exclude superconductivity as the origin for the observed negative magnetization down to ~35 K.

Reports of materials exhibiting asymmetry along the magnetization axis have been limited to a two-phase magnetic system [60]. In this case, the hysteresis loop was explained as a symmetrical α-Fe_2O_3 loop superimposed upon a very hard magnetization in one direction. This explanation cannot be applied indiscriminately to our sample because it is essentially a single-phase material.

However, $CuAl_{0.6}Fe_{1.4}O_4$ ($x = 0.6$) composition represents a complicated magnetic system. Magnetic interactions of the A-sites cations with the B-sites cations (A–B interactions) and of the B-sites cations among themselves (B–B interactions) give rise to five distinct interactions. The effects of Fe_B–Cu_B and Fe_B–Fe_B, B–B interactions have been ignored. These interactions make it possible to obtain the multiple magnetic effects required to understand the experimental results. In copper-ferri-aluminates the Fe^{3+}–O^{2-}–Fe^{3+}, A–B interaction is the strongest single interaction and will give rise to a net magnetic moment whether or not a canted spin arrangement of the Fe^{3+}-ions exists. In addition, a weaker A–B, Fe^{3+}–O^{2-}–Cu^{2+} interaction exists as well as a direct B–B, Cu^{2+}–Cu^{2+} interaction. If these latter two interactions are of comparable magnitude, the Cu^{2+} ions will have a canted spin arrangement with a net magnetic moment. This copper moment, with a net effect antiparallel to that of the Fe^{3+} ions but with different temperature dependence, could give rise to a compensation effect. However, despite the simplifications, the above description should be illustrative of the true behavior of the sample. As discussed earlier, for $NiAl_xFe_{2-x}O_4$ spinel ferrite system annealed at the rate of 1°/min, compositions with $x \geq 0.63$ have shown reversal in the direction of the resultant magnetization [70]. These results are consistent with present findings. The possibility of the presence of uncompensated spins at grain boundaries of polycrystalline sample [71], or the crystallographic imperfections cannot be neglected as a possible cause for negative magnetization.

(ii) For all the four compositions, $x = 0.0$, 0.2, 0.4 and 0.6, as the temperature decreases, the ZFC curve splits from the FC one below T_{irr}, abruptly falls below T_s' and finally saturates at T_F (Fig. 4). Such anomaly at T_s' and T_F on the ZFC curve was observed earlier in $CoCr_2O_4$ and $MnCr_2O_4$ spinels [60]. On the similar line of argument

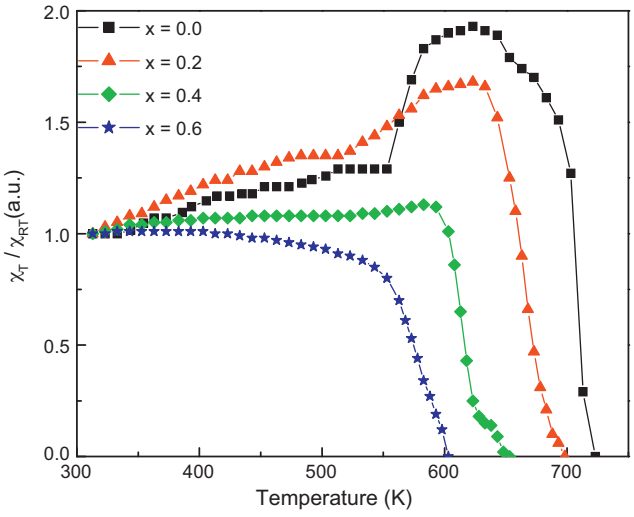

Fig. 5. Temperature dependence of ac susceptibility $\chi_{ac}(T)/\chi_{ac}(R_T)$ for different compositions of $CuAl_xFe_{2-x}O_4$ system.

in copper–ferrite–aluminates, magnetic order consists coexistence of a ferrimagnetic long range order and short range order [70], at all temperatures below the Neel temperature (T_N) up to T_{irr}. The short range order transforms into long-range at T_s' while below T_F the ferrimagnetic long–range order and the short range order coexist. The low temperature neutron scattering, specific heat and dielectric measurements are essential to understand the low temperature anomaly in the system.@@

The temperature dependence of relative ac susceptibility, $\chi_{ac}(T)/\chi_{ac}(R_T)$ ($\chi_{ac}(T)$) for all the four compositions is shown in Fig. 5. For $x = 0.0$, 0.2 and 0.4 compositions the $\chi_{ac}(T)$ displays two peaks. The first asymmetric peak at a high temperature corresponds to ferrimagnetic to paramagnetic transition temperature. The emergence of the peak just below the transition temperature can be explained based on the fact that, at lower temperature a higher value of magnetization is expected in ferrimagnetic system due to an ordering of spins within the domains. On the other hand, magnetic hardness also increases because of domain wall pinning mechanism at lower temperature. Both the competing agencies result in a peak near the transition temperature. The second lower temperature peak has the shape, which is rather like a hump, which is an indication of some degree of magnetic ordering or net result of competing anisotropies. Such a 'cusp' in susceptibility resembles the feature shown by spin glasses [72,73] and spin-glass-like phases. However, such a feature also arises due to locally canted spins system [74–76]. The second peak arises where magneto crystalline anisotropy constant changes its sign. The temperature at which the sign reversal occurs is referred to as an isotropic point. Below this temperature shape anisotropy dominates and coercive force increases rapidly resulting in a rapid diminution of susceptibility.

We see that the ferrimagnetic peak gradually diminishes on Fe-dilution indicating shift towards lower temperature and decrease in T_N. However, low temperature broad hump appears around the same temperature for $x = 0.0$, 0.2 and 0.4 compositions. The sample with $x = 0.6$ shows normal ferrimagnetic behavior.

In general, the observed features of ac susceptibility curves arise in the systems with high concentration of anisotropy ions like Co^{2+}, Mn^{3+}, Fe^{2+} as they can give rise to a local induced anisotropy. It has been shown that the system under investigation possesses small concentration of anisotropy ion Fe^{2+}.

The possibility of any spin-glass-like phase is thus ruled out based on the above discussion and the following facts:

(i) It is well known that when ferrites are sufficiently diluted with non-magnetic cations they can show a wide spectrum of magnetic structure [74]. According to Scholl and Binder [77] if the magnetic ion concentration on the A-sites and B-sites is lower than the A-sub-lattice percolation threshold (0.429) and the B-sub-lattice percolation threshold (0.390) respectively, no long range ordering is possible in the system. However, if we assume that the short range interactions are present and these are limited to the first neighbours, then according to mean field theory, the interacting spins form clusters which behave as single entities below a certain temperature. These clusters may not have the collinear spin configuration within, as the nearest neighbours are at random.

In the present system, magnetic ion concentration on both the sites is well above the percolation threshold limits thus; spin-glass-like phases cannot be expected.

(ii) If the canting angle is greater than 60°, it is expected that a transverse component is much larger than a longitudinal component. As a result there is a gradual increase of spin-spin correlation as the temperature is lowered and that favours cluster spin glass type magnetic ordering [78,79].

The canting angle is much smaller than 60° (Table 1) that prevents formation of spin-glass-like phases in the system.

(iii) On increasing the applied frequency, peak and hump temperatures should shift towards lower temperature side, which is a general feature of the cluster spin glass type of magnetic ordering.

No such shifting in peak and hump temperatures have been observed on increasing the frequency to ~1300 Hz (not shown). Thus, the possibility of spin glass type of magnetic ordering is ruled out.

(iv) If the system approaching the cluster spin glass type of magnetic ordering, sudden rise in $\chi_{ac}(T)$ with magnetic dilution has been observed [80,81], this is because of the inter-cluster interaction comparable to the thermal energy. As a result, there may be a rapid increase in magnetic viscosity resulting in the freezing of clusters.

The system studied shows no sudden rise in $\chi_{ac}(T)$ curves on magnetic dilution by replacing of magnetic (Fe^{3+}) ions by non-magnetic (Al^{3+}) ions. This further supports the absence of spin glass type magnetic ordering.

(v) If the observed magnetic moment is much lower than the spin only moments of constituent cations, one can expect that no long range ordering contributes to transverse component but it exists only for the longitudinal component. This supports the random freezing of 'spin clusters' in the system, rather than freezing of individual spins as in the case of conventional spin glass [82].

The present system showed magnetic moment for different compositions not very much lower than the Neel's moment. Thus, the possibility of spin glass type magnetic ordering is ruled out.

The magnetic transition temperature, i.e. Neel temperature (T_N), at which the magnetic susceptibility vanishes, is determined from the thermal variation of ac susceptibility measurements for different compositions as listed in Table 2. Copper ferrite is ferrimagnetic at room temperature with Neel temperature of 738 K [3], although lower values down to 290 K have also been reported [2]. The Neel temperature ~733 K found for $CuFe_2O_4$ ($x = 0.0$) (Table 2) lies in the expected range.

Table 2
Neel temperature (T_N) for $CuAl_xFe_{2-x}O_4$ system.

Al^{3+}-content (x)	Neel temperature, T_N (K)	
	ac susceptibility ±2 K	Theoretical
0.0	733	–
0.2	693	698
0.4	653	654
0.6	613	610

Table 2 shows the Neel temperature decreases with increasing Al^{3+}-content (x) in the system. The Neel temperature depends on the active magnetic linkages per magnetic ion per formula unit. The substitution of non-magnetic Al^{3+} ions (0 μ_B) for magnetic Fe^{3+} ions (5 μ_B) in the system weakens the Fe^{3+}–O^{2-}–Fe^{3+} super exchange linkages and hence the Neel temperature.

The Neel temperatures have also been calculated theoretically for $x = 0.0$–0.6 compositions, applying the modified molecular field theory [83] and using the cation distribution found from X-ray diffraction line intensity calculations. The average number of magnetic interactions, $n(x)$, for a ferrite with non-magnetic substitution (x) is given by:

$$n(x) = \frac{1}{N}[f_t f_0(Z_{BA}C_0 + Z_{AB}C_t)] \quad (4)$$

where f_t and f_0 are the fractions of magnetic concentration with respect to un-substituted ferrite and C_t and C_0 are the number of metal ions at the tetrahedral and octahedral sites respectively, Z_{BA} and Z_{AB} denote the A-site nearest neighbours to the B-site, and the B-site nearest neighbour to the A-site respectively. N is the total number of magnetic ions in a substituted ferrite. In $CuFe_2O_4$, each iron ion at the A-site is surrounded by 12 octahedral ions (Z_{AB}) on the other hand, each iron ion at the B-site has only 6 A-nearest neighbours (Z_{BA}). Thus, Eq. (4) reduces to:

$$n(x) = \frac{24}{N}(f_t f_0) \quad (5)$$

The influence of Al^{3+}-ion substitution upon Neel temperature of un-substituted ferrite $CuFe_2O_4$ may be approximated through its effect upon the average number, $n(x)$ of the super exchange interactions per magnetic ion per formula unit. In the case of $M'_{1-x}M''_xFe_2O_4$ (where M′ and M″ are non-magnetic divalent cations), there are 24/2 interactions per magnetic ion Fe^{3+} which is denoted by n ($x = 0$). In the present case, the un-substituted ferrite possesses three magnetic cations ($Cu^{2+} + 2Fe^{3+}$) with magnetic moment; Cu^{2+} (1 μB) and Fe^{3+} (5 μB). The introduction of non-magnetic Al^{3+}-ions into $CuFe_2O_4$ will reduce $n(x = 0)$, which is expressed by general chemical formula of spinel ferrite system under investigation: $CuAl_xFe_{2-x}O_4$ and Eq. (5), as:

$$n(x) = \frac{24}{1 + 5(2 - x)}[f_t f_0]$$

Therefore, the Neel temperature of Al^{3+}-substituted $CuFe_2O_4$, $T_N(x)$, will vary approximately as $n(x)$, so that it can be related to the Neel temperature of $CuFe_2O_4$, $T_N(x = 0)$, by:

$$T_N(x) = \frac{n(x)}{n(x = 0)} T_N(x = 0) \quad (6)$$

The Neel temperatures estimated using Eq. (6) for $x \leq 0.6$ compositions are in good agreement with the measured values and given in Table 2. The difference observed between measured and calculated Neel temperature values is due to the random variation of number of super exchange interactions per magnetic ion because of the random distribution of Al^{3+}-ions at the A- and B-sites.

4. Conclusions

From the aforementioned X-ray powder diffraction, field dependent magnetization $M(H)$, dc magnetization ($M(T)$) and ac susceptibility $\chi_{ac}(T)$ measurements on $CuAl_xFe_{2-x}O_4$ spinel ferrite system, several important experimental conclusions are listed below:

(1) $M(H)$ curves show high field slope, negligible coercive field and remanence. These results suggest that the materials under study are low anisotropic materials with canted spin structure.
(2) The flat response of the FC magnetization with temperature, relatively small difference in the FC and ZFC magnetization, a very broad maximum in vicinity to bifurcate temperature and a broad hump in ac susceptibility curves are characteristic features of a low anisotropy material. The observed features in ac susceptibility and dc magnetization may arise in locally canted spins system from magnetic domain effect but not due to cluster spin glass phase in the system.
(3) The composition with $x = 0.2$ shows a bifurcation between the FC and ZFC curves for the whole temperature range which indicates that the composition is not magnetically homogeneous although the material is chemically homogeneous. The negative magnetization below 35 K for $x = 0.6$ composition is due to the copper ion moment, with a net effect antiparallel to that of the Fe^{3+} ions with different temperature dependence giving rise to a compensation effect.
(4) The anomaly at T_s' and T_F on the ZFC curves for all the compositions is due to coexistence and interplay between the ferrimagnetic long range ordering and short range ordering in the system.

Acknowledgment

One of the authors (KBM) is thankful to UGC-New Delhi, for UGC – research award – 2009.

References

[1] G.F. Goya, H.R. Rechenberg, J.Z. Jiang, J. Appl. Phys. 84 (2) (1998) 1101–1108.
[2] M.U. Rana, M.Ul. Islam, T. Abbas, Solid State Commun. 126 (2003) 129–133.
[3] Ch. Venkateshwarlu, D. Ravinder, J. Alloys Compd. 426 (2006) 4–6.
[4] V.V. Parfnov, R.A. Nazipov, Inorg. Mater. 38 (1) (2002) 78–82.
[5] A. Yang, Z. Chen, S.M. Islam, C. Vittoria, V.G. Harris, J. Appl. Phys. 103 (2008), 07E509(1-3).
[6] Xu. Zuo, A. Yang, C. Vittoria, V.G. Harris, J. Appl. Phys. 99 (2006), 08M909(1-3).
[7] K.G. Saija, U.S. Joshi, V.K. Lakhani, K.B. Modi, J. Phys. D: Appl. Phys. 42 (2009), 165402 (5 pp.).
[8] J. Darul, Z. Kristallogr. Suppl. 30 (2009) 335–340.
[9] A. Yang, Z. Chen, Xu. Zuo, D. Arena, J. Kirkland, C. Vittoria, V.G. Harris, J. Appl. Phys. 86 (2005), 252510(1-3).
[10] M.M. Ibrahim, M.S. Seehra, G. Srinivasan, J. Appl. Phys. 75 (1994) 6822–6824.
[11] M. Desai, S. Prasad, N. Venkataramani, I. Samajdar, A.K. Nigam, R. Krishan, J. Appl. Phys. 91 (4) (2002) 2220–2227.
[12] M. Sultan, R. Singh, Mater. Lett. 63 (21) (2009) 1764–1766.
[13] D. Thapa, N. Kulkarni, S.N. Mishra, P.L. Paulose, P. Ayyub, J. Phys. D: Appl. Phys. 43 (2010), 195004 (5 pp.).
[14] M.A. Gabal, Mater. Lett. 64 (17) (2010) 1887–1890.
[15] S.A. Mazen, N.I. Abu-Elsaad, J. Magn. Magn. Mater. 36 (5) (2010) 1597–1601.
[16] B.S. Randhawa, H.S. Dosanjh, M. Kaur, Ceram. Int. 35 (3) (2009) 1045–1049.
[17] N.M. Deraz, J. Alloys Compd. 501 (2) (2010) 317–325.
[18] T.G. Altincekic, I. Boz, A. Baykal, S. Kazan, R. Topkaya, M.S. Toprak, J. Alloys Compd. 493 (1–2) (2010) 493–498.
[19] P.P. Kankare, M.R. Kadam, R.P. Patil, K.M. Garadkar, R. Sasikala, A.K. Tripathi, J. Alloys Compd. 501 (1) (2010) 37–41.
[20] P.V. Reddy, J. Appl. Phys. 63 (1998) 3783–3785.
[21] V.K. Lakhani, T.K. Pathak, N.H. Vasoya, K.B. Modi, Solid State Sci., doi:10.1016/j.solidstatesciences.2010.12.023.
[22] K.B. Modi, H.H. Joshi, R.G. Kulkarni, J. Mater. Sci. 31 (1996) 1311–1317.
[23] U.V. Chhaya, R.G. Kulkarani, Mater. Lett. 39 (1999) 91–96.
[24] K.G. Saija, K.B. Modi, Unpublished work.
[25] M. Almokhatar, A.M. Abdalla, M.A. Gaffar, J. Magn. Magn. Mater. 272–276 (2004) 2216–2218.
[26] R.G. Kulkarni, B.S. Trivedi, H.H. Joshi, G.J. Baldha, J. Magn. Magn. Mater. 159 (1996) 375–380.
[27] I. Maghsoudi, M.J. Hadianfard, H. Shokrollahi, J. Alloys Compd. 481 (1–2) (2009) 539–542.
[28] B.S. Trivedi, R.G. Kulkarni, Solid State Commun. 86 (1993) 327–331.
[29] M.M. Eltabey, K.M. El-Shokrofy, S.A. Gharbia, J. Alloys Compd. 509 (5) (2011) 2473–2477.
[30] S.S. Ata-Allah, M. Kaiser, J. Alloys Compd. 74 (2009) 303–309.
[31] S.M. Patange, S.E. Shirsath, K.S. Lohar, S.S. Jadhav, N. Kulkarni, K.M. Jadhav, Physica B: Condens. Matter 406 (3) (2011) 663–668.
[32] V.K. Lakhani, K.B. Modi, Solid State Sci. 12 (2010) 2134–2143, and references therein.
[33] P.A. Joy, P.S. Anil Kumar, S.K. Date, J. Phys. Condens. Matter 10 (1998) 11049–11054.
[34] J. Perez, J. Garcia, J. Blasco, J. Stankiewicz, Phys. Rev. Lett. 80 (1998) 2401–2404.
[35] K. Binder, A.P. Young, Rev. Mod. Phys. 58 (1986) 801–976.
[36] J.A. Mydosh, Spin Glasses, Taylor and Francis, London, 1993.
[37] J.E. Gareedan, N.P. Raju, A. Maigna, Ch. Simon, J.S. Pederson, A.M. Niraimathi, E. Gmelin, M.A. Subramaniam, Phys. Rev. B 54 (1996) 7189–7200.
[38] S. Pechev, B. Chevalier, D. Lattargne, B. Darriet, T. Roisnel, J. Etourneeu, J. Magn. Magn. Mater. 191 (1999) 282.
[39] P.S. Anil Kumar, P.A. Joy, S.K. Date, J. Phys. Condens. Matter 10 (1998) L487–L493.
[40] N. Kumar, A. Sundarsen, Solid State Commun. 150 (25–26) (2010) 1162–1164.
[41] P.S.R. Murthy, K.R. Pirolkar, P.A. Bhose, A. Das, P.R. Sarode, A.K. Nigam, J. Magn. Magn. Mater. 322 (22) (2010) 3704–3709.
[42] S.M. Amit Kumar, L. Yusuf, J.V. Keller, Yakhmi, Phys. Rev. Lett. 101 (2008), 207201(1-4).
[43] S.N. Dolia, J. Phys.: Conf. Ser. 200 (2010), 072026(1-4).
[44] N. Novosel, D. Pajie, A.T. Raghavender, K. Zadro, K.M. Jadav, J. Phys.: Conf. Ser. 200 (2010), 072070(1-4).
[45] M. John Jacob, Abdul Khadar, J. Appl. Phys. 107 (2010), 114310-1–114310-10.
[46] P.S. Anil Kumar, P.A. Joy, S.K. Date, Bull. Mater. Sci. 23 (2) (2000) 97–101.
[47] H. Bhargava, N. Lakshmi, V. Sebastian, V.R. Reddy, K. Venugoplan, A. Gupta, J. Phys. D: Appl. Phys. 42 (2009), 245003 (8 pp.).
[48] B.S. Trivedi, N.N. Jani, H.H. Joshi, R.G. Kulkarni, J. Mater. Sci. 35 (2000) 5523–5526.
[49] S.S. Ata-Allah, Mater. Chem. Phys. 87 (2004) 378–386.
[50] S.S. Ata-Allah, M.K. Fayek, H.S. Refai, M.F. Mostafa, J. Solid State Chem. 149 (2000) 434–442.
[51] V.K. Lakhani, K.B. Modi, J. Phys. D: Appl. Phys. (communicated).
[52] C.R.K. Murthy, S.D. Likhite, P. Sashrabudhe, Proc. Ind. Acad. Sci. 87A (1978) 245.
[53] B.H. Toby, Powder Diff. 21 (1) (2006) 67–70.
[54] M.J. Buerger, Crystal Structure Analysis, Wiley, NY, 1960.
[55] R.R. Heikes, in: R.R. Heikes, R.W. Ure (Eds.), Thermoelectricity, Wiley International, New York, 1961.
[56] R.M. Persoons, E. de Grave, P.M.A. de Bakker, R.E. Vandenberghe, Phys. Rev. B 47 (1993) 5894–5905.
[57] B.C. Zhao, H.W. Hu, B. Xia, L.H. Tan, A.C. Huan, L. Wang, Appl. Phys. Lett. 93 (2008) 222506–222509.
[58] L. Néel, Ann. Phys. 3 (1948) 137–142.
[59] A. Rosencwaig, J. Phys. 48 (1970) 2857–2867.
[60] N. Menyuk, K. Dwight, D.G. Wickham, Phys. Rev. Lett. 4 (3) (1960) 119–120.
[61] V.I. Trukhin, V.I. Maksimochkin, Yu.A. Elesin, V.A. Zhilyaeva, Moscow Univ. Phys. Bull. 62 (1) (2007) 51–57.
[62] K. Tomiyasu, J. Fukunaga, H. Suzuki, Phys. Rev. B 70 (2004), 214434(1-12).
[63] L. Wang, J. Ding, A. Roy, J. Ghose, Y. Li, Y.P. Feng, J. Phys. Condens. Matter 12 (2000) 9963–9972.
[64] V.A. Khomchenko, I.O. Troyanchuk, R. Szymczak, J. Mater. Sci. 43 (2008) 5662–5665.
[65] O. Kahn, Nature (London) 399 (1999) 21–22.
[66] Yu.G. Chukalkin, V.R. Shtirts, Phys. Stat. Sol. A 173 (2) (1999) 459–465.
[67] R.P. Singh, C.V. Tomy, J. Phys. Condens. Matter 20 (2008) 235209 (7 pp.).
[68] C. Mathoniere, C.J. Nuttall, S.G. Carling, D. Peter, Inorg. Chem. 35 (5) (1996) 1201–1206.
[69] M.M. Ibrahim, M.S. Seehra, J. Appl. Phys. 75 (10) (1974) 6822–6824.
[70] L.R. Maxwell, S.J. Pickart, Phys. Rev. 92 (5) (1953) 1120–1126.
[71] G. Lawes, B. Melot, K. Page, C. Ederer, M.A. Hayward, Th. Proffen, R. Seshadri, Phys. Rev. B 74 (2006), 024413-1–024413(1-6).
[72] C.Y. Huang, J. Magn. Magn. Mater. 51 (1985) 1–74.
[73] J.L. Soubeyroux, D. Fiorani, E. Agostinelli, J. Magn. Magn. Mater. 54 (1986) 83–84.
[74] J.L. Dormann, M. Nogues, J. Phys. Condens. Matter 2 (1990) 1223–1237.
[75] S.M. Yusuf, V.C. Sahni, L. Madhav Rao, J. Phys. Condens. Matter 7 (1995) 873–881.
[76] S.M. Yusuf, L. Madhav Rao, PRAMANA-J. Phys. 47 (1996) 171–182.
[77] F. Scholl, K. Binder, J. Phys. B 39 (1980) 239–247.
[78] R.B. Jotania, R.V. Upadhyay, R.G. Kulkarni, IEEE Trans. Magn. 28 (4) (1992) 1889–1894.
[79] J. Nogues, T. Puig, R.B. Jotania, R.V. Upadhyay, R.G. Kulkarni, K.V. Rao, J. Magn. Magn. Mater. 99 (1991) 275–279.
[80] B.S. Trivedi, PhD thesis, Saurashtra University Rajkot, India, 1993.
[81] K.B. Modi, PhD thesis, Saurashtra University Rajkot, India, 1996.
[82] K.B. Modi, H.H. Joshi, R.G. Kulkarni, Ind. J. Pure Appl. Phys. 34 (1996) 92–95.
[83] G.J. Baldha, R.V. Upadhyay, R.G. Kulkarni, J. Mater. Sci. 23 (1988) 3357–3361.